

RESEARCH ARTICLE

The multistep decomposition of boric acid

Clemens Huber¹  | Saman Setoodeh Jahromy¹  | Felix Birkelbach²  |
 Jakob Weber¹ | Christian Jordan¹ | Manfred Schreiner³  | Michael Harasek¹  |
 Franz Winter¹ 

¹Institute of Chemical, Environmental and Bioscience Engineering, TU Wien, Vienna, Austria

²Institute for Energy Systems and Thermodynamics, TU Wien, Vienna, Austria

³Institute for Natural Sciences and Technology in the Arts, Academy of Fine Arts Vienna, Vienna, Austria

Correspondence

Clemens Huber, Institute of Chemical, Environmental and Bioscience Engineering, TU Wien, Getreidemarkt 9/166, 1060 Vienna, Austria.
 Email: clemens.huber@tuwien.ac.at

Funding information

Austrian Research Promotion Agency (FFG), SolidHeat Pressure (#853593), SolidHeat Kinetics (#848876) and SolidHeat Basic (#841150).

Abstract

Due to its high potential for thermal energy storage systems (Huber, Setoodeh Jahromy, Jordan, et al, *Energies*. 2019;12:17) the decomposition of boric acid is of particular interest in the field of applied research. The complexity of the reaction mechanism, with its multiple partial-overlapping reaction steps, hitherto prevented a clear identification and analysis of each stoichiometric reaction step. So far, various research teams performed different kinetic analyses of boric acid, which led to various reaction mechanisms and stoichiometric reaction steps with yet inconclusive results for process modeling. Thus, a deeper examination of the process was desirable, to validate whether a proposed reaction is reasonable or not. For this purpose, experimental data were used for a deconvolution of the reaction sequence, using the Fraser-Suzuki function, which clearly revealed the respective single reactions. The results of the deconvolution were compared with the proposed reaction steps in consideration of the stoichiometric ratio and thereby illustrated that the decomposition of polycrystalline boric acid more likely consists of three reaction steps. In contrary to the two-step mechanism, the three-step mechanism showed a very good correlation ($r > 99\%$). Based on these outcomes, kinetic analyses were performed for each reaction step, by means of the nonparametric kinetics 2 (NPK2) method with subsequent determination of kinetic parameters. Additionally, for a deeper insight into the reaction, analyzing techniques like X-ray diffraction (XRD), scanning electron microscopy (SEM) and simultaneous thermal analysis (STA) were applied.

KEYWORDS

boric acid, deconvolution, Fraser-Suzuki, nonparametric kinetics, thermal energy storage, thermogravimetric analysis, waste heat trading

1 | INTRODUCTION

Based on renewable energy sources, thermochemical energy storages are considered as a high potential and crucial

technology to not only reduce the dependency on fossil fuels, but also to ensure the energy supply for the future. The ecological footprint, a measure indicating the human demand on nature, illustrates the actual problem as well as the need

This is an open access article under the terms of the Creative Commons Attribution License, which permits use, distribution and reproduction in any medium, provided the original work is properly cited.

© 2020 The Authors. *Energy Science & Engineering* published by the Society of Chemical Industry and John Wiley & Sons Ltd.

for a global change. At present, the annual need of resources exceeds an equivalent of 1.7 earths, meaning, that the earth would need 1 year and 6 months to regenerate from 1 year of human exploitation.¹ With respect to energy, the expected global energy demand will rise by 30%, associated with a slight increase of energy-related CO₂ emissions until the year 2040.² This forecast clearly demonstrates the importance of CO₂-free—renewable—energy sources without further impact on the ecological footprint. The severe consequences of the steadily rising air pollution from greenhouse gas emissions, such as rising sea levels, droughts, floods, or hurricanes, are omnipresent all around the globe. At an event on “Clean Industrial Revolution” in Duran on the 6th of December 2011, former UN Secretary-General Ban Ki-moon emphasized the need to tackle the danger of climate change caused by fossil fuels and further highlighted the importance of a sustainable energy provision.³

Most renewable energy sources share a common drawback, the unsteady supply of energy, depending on different influencing factors like daytime, season, location, or weather. Energy storage technologies can be considered as suitable tools to bridge the decisive gap, between times of energy supply and actual energy demand.

Solar thermal energy plants, for example, could clearly benefit from thermal energy storage (TES) systems. Combining these both technologies would considerably enhance the efficiency of energy generation and enable new operational functions. The facilitation of baseload energy generation by solar energy or a guaranteed energy provision, even during peak times of energy demand, independent of actual weather conditions are only two corresponding benefits.⁴

A further potential field of application for TES systems would be the economic utilization of waste heat. Instead of using other nonrenewable energy sources, waste heat can work as a suitable alternative to meet the energy needs of consumers, by simultaneously preventing the emergence of new harmful emissions. Primary requirement for waste heat trading (“waste heat exchange”) and the utilization of waste heat would be the decoupling of energy production via TES systems (heat supply) and energy demand.

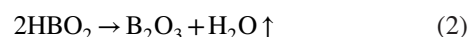
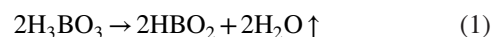
Thermal energy storage systems are divided into sensible, latent, and chemical energy systems. Among these, thermochemical energy systems have the highest thermal energy density, are capable of storing energy for long periods with very low heat losses, and are therefore of particular scientific interest.⁵ So far, boric acid and boron oxide have already been used for a broad range of applications and products such as ceramics, detergents fertilizers, glass, mineral wool, sport equipment, insecticides, or medical treatments.⁶⁻⁹ However, recently, the boric acid-boron oxide system received further attention as a promising candidate for storing thermal energy.¹⁰ Its high-energy density of

2.2 GJ/m³ could meaningfully contribute to the global sustainable energy supply.

For the development of a TES process, it is indispensable to study the chemical reaction characteristics such as reversibility, rate of reaction, or its kinetic properties.¹¹ Due to its large area of application, the boric acid-boron oxide system has already been well researched during the first half of the 20th century. Various studies are therefore already engaging with its properties like solubility, hardness, volatility, crystal structure, or other technical relevant physical characteristics.¹²⁻¹⁷ Although kinetic analyses have been conducted as well, the complexity of this reaction leads to varying results within the analyses, which is why the mechanism is not yet clearly identified. The consequence is still a lack of essential information regarding the detailed sequences, of the physical and chemical reaction steps.¹⁸

The dehydration of boric acid to boron oxide is a multistep reaction, consisting of various—at least two—consecutive reaction steps with partially overlapping areas. In literature, two different approaches for the reaction mechanism have been described so far, using a thermogravimetric analysis under nonisothermal conditions.

Sevim et al¹⁹ evaluated the kinetics of the boric acid dehydration reaction, assuming a two-step reaction (1) and (2). Following this assumption of two distinct steps, further kinetic analyses, without a clear separation of these steps, were performed by Balci et al²⁰ and Zhang et al²¹



While examining different crystalline structures of boric acid, Harabor et al,²² however, observed three different thermal-induced reaction steps (3)–(5). The mass loss was attributed to each of this reaction steps. Based on this result, the kinetic analysis of Rotaru²³ and Aghili et al²⁴ confirmed three distinct steps. Their experimental work, though, was not able to provide complete results for each of these steps because of a missing clear step separation. In 1978, it was already described that the “new” intermediate H₂B₄O₇ was part of the boric acid decomposition.²⁵ Table 1 gives a summary of hitherto performed kinetic analyses on that reaction.

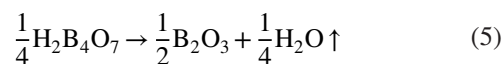
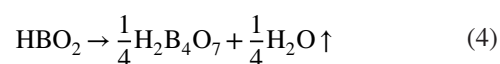
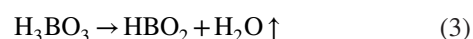


TABLE 1 Comparison between the kinetic analyses of boric acid since 2006: parameter and results

Source	<i>m</i> mg	Gas mL/min	HR °C/min	<i>T</i> _{MAX} °C	Step	<i>E</i> _a kJ/mol	<i>A</i> min ⁻¹	Model
Sevim et al ¹⁹	20	N ₂ 25	3	600	1 2	79.85 4.79	3.8 × 10 ⁴ 4.1 × 10 ⁻⁵	F1 F1
Balcı et al ²⁰	5000	Air 75	5 dwells: 30' at 130°C, 60' at 330°C	450	1 2	45 24	1.1 × 10 ¹ 3.4 × 10 ⁻²	F1 F1
Zhang et al ²¹	20	N ₂ 30	3, 5, 10, 20	800	1 2	143.92 69.9	1.9 × 10 ¹⁶ 1.5 × 10 ⁷	D4 D3
Rotaru ²³	1.3-2.2	Air 150	2, 4, 6, 8	500	1 2 3	~175-115 (TBA)/~80 (HBA) ~155-80 (TBA)/~100-80 (HBA) 80-190 (TBA)/150 (HBA)	n.a. n.a. n.a.	n.a. n.a. n.a.
Aghili et al ²⁴	10.5	Ar n.a.	3, 5, 10	600	1 2 3	55 n.a. n.a.	5.7 n.a. n.a.	A2 n.a. n.a.

Note: Sample mass (*m*), gas flow (Gas), heating rate (HR), activation energy (*E*_a), preexponential (frequency) factor (*A*), and model (Table 2), triclinic boric acid (TBA), hexagonal boric acid (HBA).

By using a new approach, this paper will elaborate on the reaction sequence and the global kinetics for the application of process modeling and the design of a thermochemical energy storage reactor. Other side effects of the boric acid decomposition reaction, observed in the course of the TG analysis, will be described as well. So far, the reaction's challenging characteristics, with an inconclusive number of partial-overlapping reaction steps, prevented a clear kinetic identification of the particular reaction steps, leading to different kinetic triplets. One main reason therefore could be an unclear separation of the reaction steps.²⁶ The methodology of this work thus addresses this point by combining a deconvolution of the overlapping reaction rates with an innovative kinetic modeling approach.

The deconvolution of the overall decomposition reaction rate into the respective single reaction rates was performed via the application of the Fraser-Suzuki function.²⁷ Enhancing the procedure by an evaluation of the deconvolution procedure's chemical justification ensured the results to be consistent with the respective reaction's stoichiometry.

For kinetic computations, many different methods and procedures, with different advantages depending on the application field, have so far been developed.^{26,28} In addition to this, this work uses another method, the nonparametric kinetics method (NPK2).²⁹ For applied research and the desired application, this approach was considered suitable for the subsequent kinetic analysis of the obtained individual single reaction rates. Figure 1 provides an illustration of the methodology's key steps.

This work will thus help to further elucidate the decomposition reaction inter alia by evaluating the suitability of yet proposed reaction mechanisms and by providing kinetic information for process modeling and the design of an energy storage reactor. With regard to future heat storage processes, the results will furthermore contribute to a better understanding of the boric acid decomposition reaction and encourage the optimization of the process control—like an ideal temperature profile or the avoidance of unwanted intermediate reactions like eutectic melt—toward an ideal storage process. Therefore, it will form the basis for further research and development work on this promising TES system.

2 | MATERIALS AND METHODS

Polycrystalline boric acid from Carl Roth GmbH (6943/CAS 475234072) was used for the analyses within this work. The materials' purity of more than 99%—declared by the manufacturer—was checked by means of acidimetric titration and inductive plasma spectroscopy.

The nonisothermal thermogravimetric analyses of the decomposition were performed in accordance with the recommendations of the Kinetics Committee of the International Confederation for Thermal Analysis and

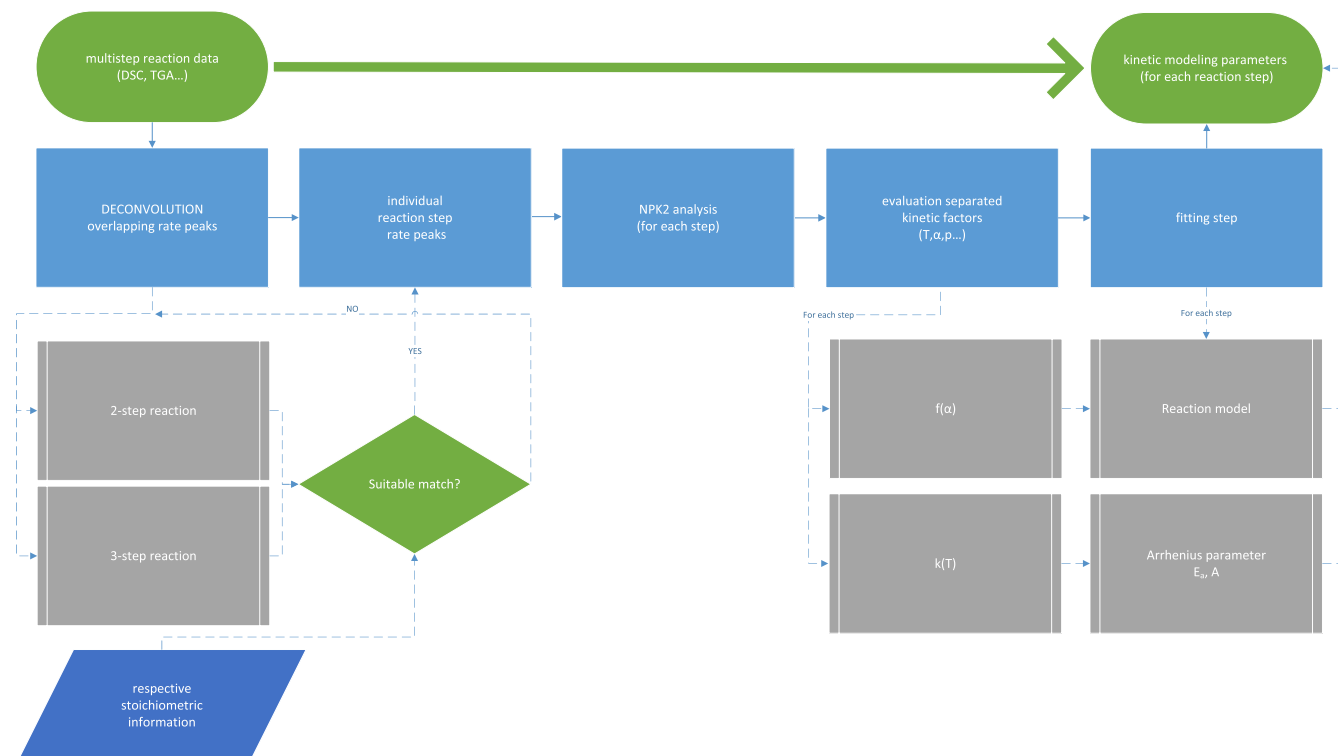


FIGURE 1 Methodology presented by the key steps sequence

Calorimetry (ICTAC), for collecting experimental thermal analysis data for kinetic computations.³⁰ To enable a moderate decomposition rate as well as an immediate removal of the evolved gas, major influencing factors on the reaction such as the sample mass, gas atmosphere, and heat need to be controlled. Consequently, within a series of kinetic measurements at different heating rates, the sample mass should be kept practically constant and as small as

TABLE 2 Important reaction models^{31,43}

Notation	$f(\alpha)$	Type
D1	$\frac{1}{2\alpha}$	1-D diffusion
D2	$-\frac{1}{\ln(1-\alpha)}$	2-D diffusion
D3	$\frac{3(1-\alpha)^{2/3}}{2[1-(1-\alpha)^{1/3}]}$	3-D diffusion-Jander
D10	$3(1-\alpha)^{4/3}$	New equation
A1	$4(1-\alpha)[- \ln(1-\alpha)]^{3/4}$	Avrami-Erofeev
A2	$2(1-\alpha)[- \ln(1-\alpha)]^{1/2}$	Avrami-Erofeev
A3	$3(1-\alpha)[- \ln(1-\alpha)]^{2/3}$	Avrami-Erofeev
A4	$4(1-\alpha)[- \ln(1-\alpha)]^{3/4}$	Avrami-Erofeev
A5	$\frac{3}{2}(1-\alpha)[- \ln(1-\alpha)]^{1/3}$	Avrami-Erofeev
F0/R1	1	Zero-order
F _n	$(1-\alpha)^n$	n^{th} order ($n > 0$)
R2	$2(1-\alpha)^{1/2}$	Contracting area
R3	$3(1-\alpha)^{2/3}$	Contracting volume
B1	$\alpha(1-\alpha)$	Prout-Tompkins

possible. When using fine powder, it is recommended to apply a thin layer of sample particles (on the pan bottom), so that they ideally react uniformly and thus, without mass influence on the reaction (mass loss curve). The experiments should be performed under an appropriate—dependent on the instrument configuration—dry inert gas flow (like nitrogen or argon), ensuring the efficient removal of the gaseous product. In general, fast heating rates should be avoided as they enhance the temperature gradient inside the sample, causing a nonuniform particle reaction and, thus, reducing the reliability of the experimental data.

2.1 | Characterization

The samples were characterized by particle size distribution (PSD), X-ray diffractometry (XRD), scanning electron microscopy (SEM), and simultaneous thermal analysis (STA).

2.1.1 | Particle size distribution (PSD)

The particle size of the sample material was analyzed by a laser diffraction measurement device (Mastersizer 2000, Malvern Instruments). This device was equipped with a dry dispersion module Scirocco 2000), for particle-in-gas sizing. It provided a particle size analysis ranging from 0.020 to 2000 μm .

2.1.2 | X-ray diffraction analysis (XRD)

The sample material was identified by powder X-ray diffraction measurements. The measurements were carried out on a PANalytical X'Pert Pro diffractometer device in Bragg-Brentano geometry. It uses a mirror for separating the Cu K α 1,2 radiation and an X'Celerator linear detector. An Anton Paar HTH1200N chamber was used for in-situ monitoring of the experiments.

2.1.3 | Scanning electron microscopy (SEM)

For a deeper insight into the sample structure, revealing possible morphological changes during the decomposition, a scanning electron microscope device (COXEM EM-30PLUS) was used for imaging the particle surface before and after the reaction.

2.2 | Simultaneous thermal analysis (STA)

The experimental investigation of the reaction was performed by a STA device (Netzsch STA449 Jupiter). This device was equipped with a TGA-DSC sample holder. The device's oven enabled experimental investigations within a positive temperature range from 25°C up to 1250°C regulated by an S-Type thermocouple. For the experiments, aluminum oxide crucibles without lids ($\varnothing = 6$ mm, 75 μ L) were used. Furthermore, mass flow meters (Red-y smart, Voegtlin) controlled the inert gas flow rate. For each experimental run, a nitrogen flow rate of 100 mL/min was set.

The dehydration process was analyzed under nonisothermal conditions (2, 4 and 8°C/min). As stated previously, according to the recommendations of ICTAC, the sample mass should be minimized to ideally obtain results uninfluenced by the mass. As a general rule, a sample mass causing a mass loss of 1 mg is recommended.³⁰ Earlier studies with various sample masses could not exclude a mass influence on the results.¹⁰ Therefore, a sample mass of 2 mg was set for all experiments.

2.3 | Theoretical

The kinetic identification of a solid-state reaction, like this decomposition reaction, without consideration of the pressure influence $h(p)$, is based on the isothermal rate equation

$$\frac{d\alpha}{dt} = k(T)f(\alpha) \quad (6)$$

where $f(\alpha)$ is the reaction model and $k(T)$ the temperature influence. This can be modeled inter alia by using the Arrhenius equation.

$$k(T) = Ae^{\left(-\frac{E_a}{RT}\right)} \quad (7)$$

yielding

$$\frac{d\alpha}{dt} = Ae^{\left(-\frac{E_a}{RT}\right)}f(\alpha) \quad (8)$$

where A is the frequency factor, T the absolute temperature, E_a the activation energy, α the extent of reaction, and R the gas constant. The frequency factor, the activation energy, and the reaction model are called the kinetic triplet and are essential results of a kinetic analysis. The definition of α for a gravimetric measurement is

$$\alpha = \frac{m_0 - m_t}{m_0 - m_\infty} \quad (9)$$

where m_0 is the initial mass, m_∞ the final weight, and m_t the mass at time t . With the heating rate (β) applied to Equation (8), gives the nonisothermal rate expression

$$\frac{d\alpha}{dT} = \frac{A}{\beta} e^{\left(-\frac{E_a}{RT}\right)}f(\alpha) \quad (10)$$

The methods for performing a kinetic analysis are divided into model fitting (preassuming a model) and model-free methods.

The reaction model is a theoretical description of the experimental results, or a so-called mathematical translation. There are various proposed reaction models, each describing a different reaction type/mechanism, either based on mechanistic assumptions or empirical derivations.³¹ The derivation of several reaction models is based on isothermal reaction conditions and oversimplified assumptions regarding the reactants structure (single crystal solids with a well-defined geometry).³¹ Possible occurring changes during the reaction, as well as effects of the generated product, are typically ignored.³² This needs to be considered when looking at the results.

2.4 | Deconvolution

For the description of the overall multistep reaction, the kinetic triplet of each individual reaction step needs to be determined. Unfortunately, common analysis methods are not capable to handle complex multistep reactions. Therefore, there is a need for new procedures enabling the kinetic analysis of each individual step of multistep processes. A promising and increasingly popular approach for the kinetic analysis of multistep reactions comprises the peak separation of each respective reaction step via peak deconvolution and subsequent kinetic analysis.³³

For the deconvolution of such reactions, statistical functions like the Lorentzian, Gaussian, Fraser-Suzuki, or Weibull function were used.³⁴⁻³⁶ Perejon et al²⁷ analyzed the suitability of different statistical fitting functions, applied to the deconvolution of complex solid-state reactions. They determined the Fraser-Suzuki function (11) as most appropriate, to fit a reaction properly and independent of the kinetic model. It enables correct parameters of the subsequent kinetic analysis although, the reaction results deviate from the kinetic model due to inhomogeneities in particle size or shape.³⁴ Generally, symmetric peak functions like Gaussian or Lorentzian are not recommended because reaction rates usually show an asymmetrical shape.³³

The Fraser-Suzuki function is given as³⁶:

$$y = a_0 \exp \left[- \ln 2 \left[\frac{\ln(1+2a_3 \frac{x-a_1}{a_2})}{a_3} \right]^2 \right] \quad (11)$$

where a_0 , a_1 , a_2 , and a_3 are parameters for the amplitude, position, half-width, and asymmetry of the curve.

The deconvolution procedure of the thermogravimetric data was performed within Python (Python Software Foundation). The thermogravimetric raw data were prepared for the deconvolution by using a Savitzky-Golay smoothing filter³⁷ and a linear baseline correction. For the distinction between the proposed reaction mechanisms, the deconvolution was performed for two and three defined reaction steps, by least square fitting to the overall reaction. To chemically justify the received results, the stoichiometric mass loss ratio of the respective steps was implemented into the algorithm, to ensure that the calculated reactions fulfill the stoichiometric condition.

2.5 | Kinetic analysis and model identification

For the kinetic modeling of the reaction steps, the refined NPK 2.0 method was used.²⁹ This method, originally described in 1998 by Serra et al,³⁸ bases on the observation that the discretization of the general kinetic equation (6) results in a rank-one matrix. By arranging the reaction's experimental data in a matrix and applying a suitable algorithm to compute its rank-1 approximation, the conversion and the temperature dependency vectors can be extracted without any assumption about the model besides the single-step approximation. The NPK method is not limited to a certain number of variables with impact on the reaction rate. For instance, it can therefore also handle the pressure dependence $h(P)$ of the reaction kinetics.³⁹

This data-driven approach is often labeled “model-free,” in the sense that no reaction model has to be chosen beforehand.⁴⁰ Models are selected and parametrized after the

separation, independently for each variable (T , α) by nonlinear least square fitting the result vector $f(\alpha)$.

Generally, this is much easier and less error-prone, compared with direct model fitting methods. To improve the quality of the model fitting step, the uncertainty of each result value was calculated and weighted accordingly. The weighted results were used for the fitting algorithm.

A simplified mathematical description for the nonlinear least square fitting problem can be given via⁴¹:

$$\min_x f(x) = \frac{1}{2} \sum_{i=1}^m f_i(x)^2 \quad (12)$$

With $f_i(x)$ as the auxiliary function (nonlinear, not arbitrary, corresponding to the residuals in general data fitting problem) and 1/2 as scaling factor.

Birkelbach et al²⁹ give a detailed description of the specific fitting procedure used for this work.

The best fitting reaction model was identified by fitting 41 reaction models from the literature to the calculated conversion dependency vector. The sum of squared errors (SSE) is the resulting sum of the squares of residuals from (nonlinear least square) fitting the result vector data to the respective reaction model. In addition, a pairwise F test was performed to check whether the performance of the best fitting model was statistically, significantly better than the others. The probability that the tested model is actually the better fitting one despite showing a higher deviation is given by the P -value. In the result plots, all models are displayed that were not rejected at a 95% confidence level ($P = .05$).

The Arrhenius parameters (E_a , A) were identified from the temperature dependency $k(T)$ with a nonlinear least square fitting algorithm. The activation energy E_a is displayed with its 95% confidence interval. Table 2 provides important reaction models.

3 | RESULTS AND DISCUSSION

3.1 | Characterization (PSD, XRD, and SEM)

Figure 2 shows the particle size analysis results of the used boric acid, the cumulative frequency (Sum), and the particle size distribution (Frequency).

The powder XRD analysis was performed with boric acid samples before and resulting boron oxide after thermal decomposition via STA analysis.

Figure 3 revealed a characteristic pattern of boric acid, whereas the analysis of boron oxide showed only a large bump without any significant peak (Figure 4). The surface morphology apparently changed during the thermal analysis, from a crystalline to an amorphous structure.

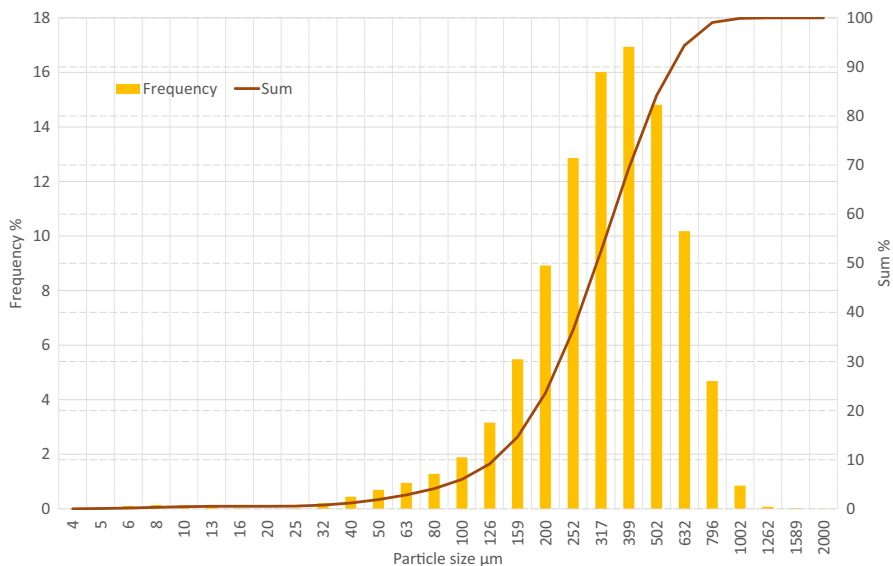


FIGURE 2 Particle size distribution of H_3BO_3

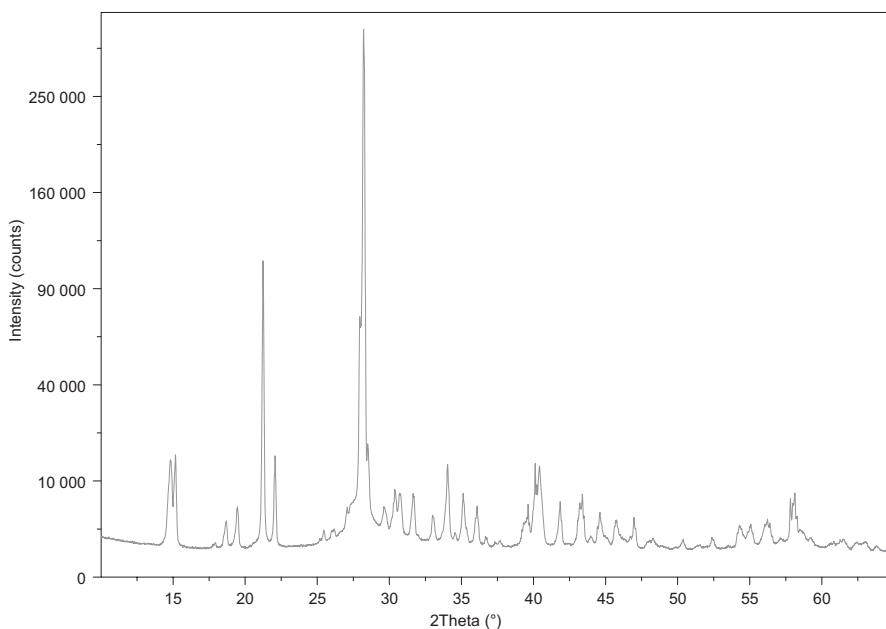


FIGURE 3 X-ray diffraction analysis of H_3BO_3 before STA analysis

The SEM images of H_3BO_3 before the thermal analysis revealed the particles round shape with a smooth, flaky surface (Figure 5). The images of the resulting B_2O_3 particles after the STA analysis showed an uneven and rough surface (Figure 6). These pictures could neither clearly confirm nor exclude a possible melting on the particle's surface.

To verify the XRD's analysis findings, an additional experiment was performed. Boric acid particles in a steel crucible were exposed (by using a muffle furnace) to a temperature ramp, similar to the ramp of the thermal analysis of $2^\circ C/min$, and kept at a temperature of $155^\circ C$ for 6 hours. During this time, the particles formed a tablet, probably due to sintering or surface melting effects (Figure 7). This happened although the temperature ramp was low, and the lowest melting point of the reaction (boric acid at $171^\circ C$) was not reached. In literature, it is described that different reactions are accompanied by melting, attributed to the

participation of an intermediate that melts either at reaction temperature or while forming an eutectic with a reactant.¹⁸

3.2 | Simultaneous thermal analysis

For the thermal analysis, boric acid with a particle size in the range of $63-125 \mu m$ was used. Figure 8 shows the STA results of the boric acid decomposition, using a sample mass of 2 mg at different heating rates. The final weight of around 56% of the original mass was consistent with the theoretical weight loss of 43.7%. This analysis was not able to provide further information concerning the apparent morphological change. Differential scanning calorimetry results could help (provided that all reaction steps and crystal changes are identified) to show possible phase changes during the reaction.

FIGURE 4 X-ray diffraction analysis of resulting B_2O_3 after STA analysis

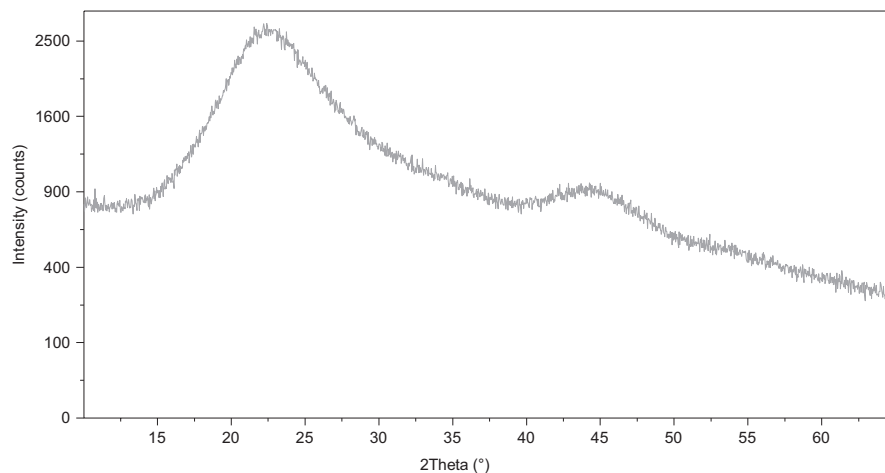


FIGURE 5 SEM images of H_3BO_3 before STA analysis: (A) 300× magnification at accelerating voltage of 20 kV and working distance of 9.9 mm; (B) 2000× magnification at accelerating voltage of 15 kV and working distance of 9.2 mm

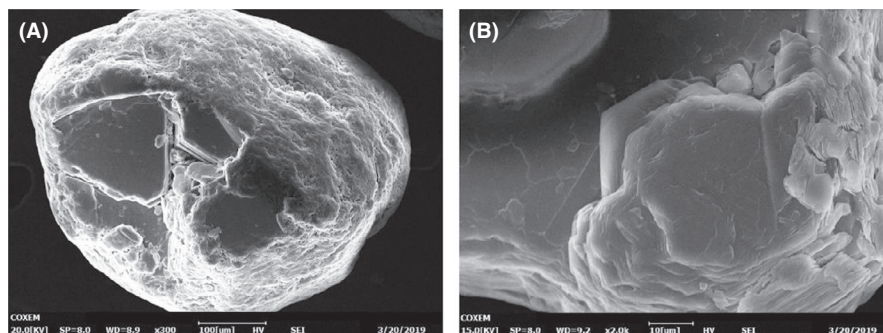


FIGURE 6 SEM images of B_2O_3 after STA analysis: (A) 1000× magnification at accelerating voltage of 10 kV and working distance of 9.2 mm; (B) 2000× magnification at accelerating voltage of 10 kV and working distance of 9.2 mm

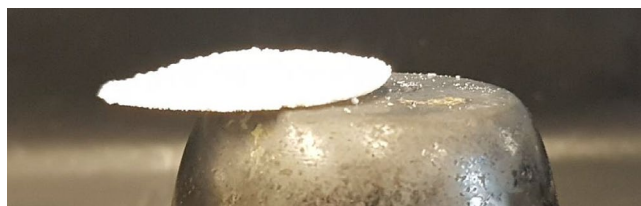
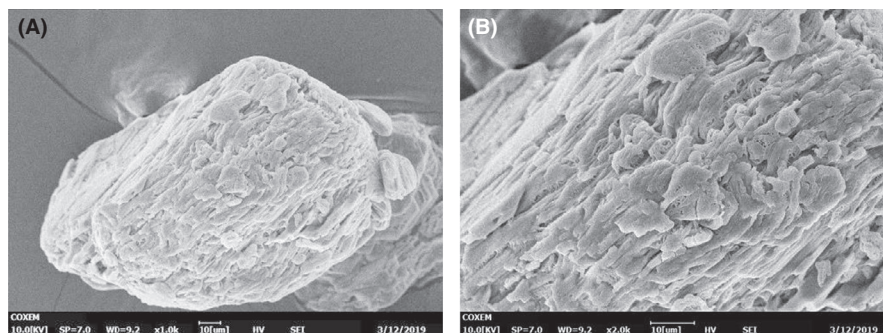


FIGURE 7 Apparent sintering effect on boric acid particles exposed to 155°C over a period of 6 h

3.3 | Deconvolution

Besides a good fitting quality, the results had to meet the stoichiometric mass loss ratio within an interval of plus/minus three percent, to interlink the mathematical results to the chemical reaction (Table 3).

3.3.1 | Two-step reaction mechanism

For a two-step reaction (5) and (6), the calculated results had to meet the reactions' stoichiometric ratios on the overall mass loss with 67% for the first and 33% for the second reaction. However, the results revealed that due to the overall reaction curve progression, it was impossible to gain a result with good quality and a matching ratio, for a two-step reaction. The dimension of the last peak (with an average ratio of about 13%) was far too small to enable the required second reaction step. Figure 9A-C, therefore, shows the best fitted results ($r > 99\%$) neglecting the stoichiometric ratio. For keeping the stoichiometric condition, the small last peak needs to be ignored. Figure 10 demonstrates the mismatch between the overall reaction curve progression and a two-step reaction mechanism, using simulated reaction curves with the

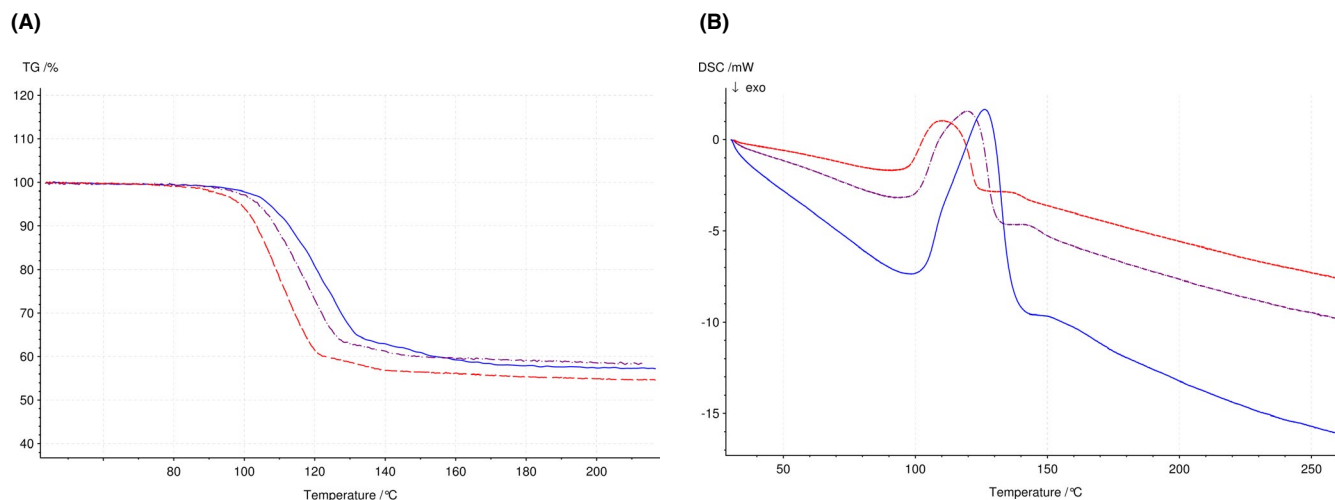


FIGURE 8 Dehydration of 2 mg H₃BO₃ at heating rates of 2 (red/dashed), 4 (violet/dash-dotted) and 8°C/min (blue/ solid) showing the reaction's mass loss (A) and specific heat flow (B). The respective temperature ramp course is presented as dotted line with the heating rate corresponding color

	Step 1	Step 2	Step 3
Two-step reaction	67%	33%	–
	2H ₃ BO ₃ → 2HBO ₂	2HBO ₂ → B ₂ O ₃	–
Three-step reaction	66%	17%	17%
	H ₃ BO ₃ → HBO ₂	HBO ₂ → $\frac{1}{4}$ H ₂ B ₄ O ₇	$\frac{1}{4}$ H ₂ B ₄ O ₇ → B ₂ O ₃

TABLE 3 Stoichiometric mass loss ratio for the respective reactions (2-step/3-step)

ideal stoichiometric ratio of 67-33 percent. Consequently, the results of the two-step mechanism were considered as inappropriate to describe the decomposition reaction and thus, refrained from a kinetic analysis.

3.3.2 | Three-step reaction mechanism

Unfolding the overall reaction into three distinctive reaction steps provided better quality results. The obtained reaction steps kept both conditions, the resulting curves had a maximum deviation of plus/minus three percent from the stoichiometric mass loss ratio, as well as a high correlation of more than 99%. Figure 11A-C shows deconvolution results for a three-step reaction of the boric acid decomposition. Regions with overlapping steps, as well as initial and end areas, revealed the biggest deviations. Due to the complex curve progression, at the beginning and the end of the overall reaction, the position of the linear baseline was responsible for deviations in initial and end areas of the reaction. It was not reasonable to apply another baseline type because of the unclear reaction progress with overlapping reaction steps. The deconvolution quality was generally suffering in areas with overlapping reaction steps. This is the case in step 2, which apparently gets influenced

by reaction step 1 and 3. Overall, it can be said that the three-step deconvolution results appear more suitable for describing the boric acid decomposition.

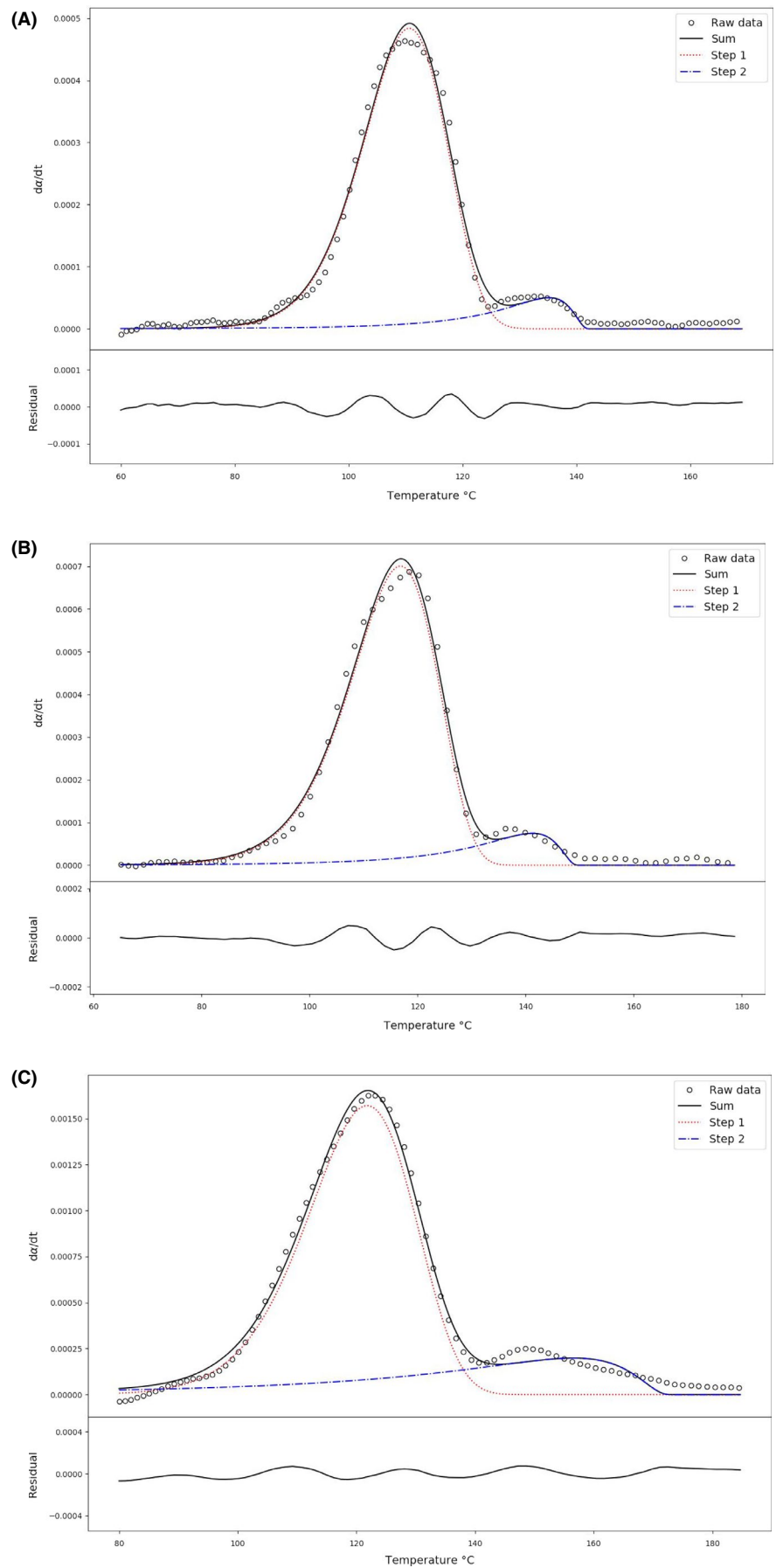
3.4 | Kinetic analysis and model identification

With the revealed three-step reaction sequence, the subsequent kinetic analysis was performed for each reaction step. The calculated reaction's conversion and the reaction rate are illustrated for step 1 (Figure 12), step 2 (Figure 13), and step 3 (Figure 14). Figures 15-17 present the analysis results for each reaction step comprising: The calculated kinetic results (from the NPK method), the respective standard deviation (error bars), the statistically most fitting reaction model as well as the temperature dependency. The related results are further listed in Table 4.

While data calculated via the NPK method for step 1 statistically fit best to one specific reaction order model (Figure 15), inaccuracies at the beginning of the reaction leave room for other equally fitting reaction models. These models are listed in Table 5.

Reaction step 2 seems to follow an Avrami-Erofeyev model (Figure 16) for nucleation/ nuclei growth. Although the reaction seems to be influenced by the first and the last

FIGURE 9 Deconvolution results assuming a two-step reaction; ratios of step 1 and step 2 for a heating rate of: 2°C/min 91:9% (A), 4°C/min 90:10% (B) and 8 C/min 80:20% (C)



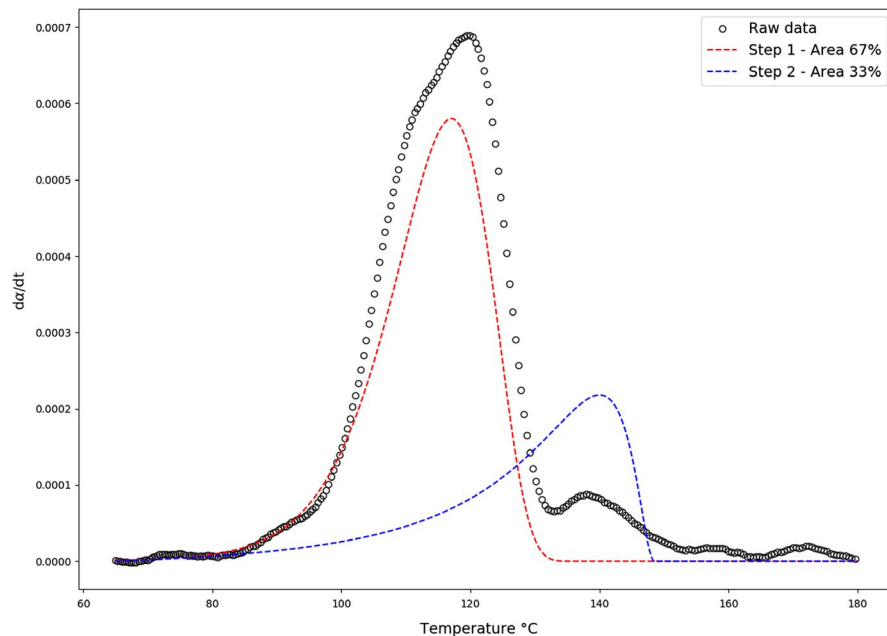


FIGURE 10 Deconvolution results assuming a two-step reaction; ratios of step 1 and step 2 for a heating rate of 4°C/min using the theoretical ideal stoichiometric ratio (67:32%)

reaction step, causing the slight oscillating temperature dependency shape, the reactions temperature dependency follows the exponential trend of the Arrhenius equation. For the sake of completeness, Table 6 lists further potential fitting models.

The progression of reaction step 3 statistically fits best to a diffusion-derived model, and the reactions temperature dependency is following the Arrhenius equation (Figure 17). The statistic performance of other well-fitting models is listed in Table 7.

The P -value is the probability in the F test that the tested model is actually the better fitting one, even though it shows a higher deviation. For values of $.5 > P > .05$, there is no significant statistical difference between the best fitting model and the tested one. Thus, it is not the case that the tested model, showing a higher deviation, is better than the best fitting model (null hypothesis rejected). For $P < .05$, the best fitted model is significant statistical better than the tested model.

4 | CONCLUSION

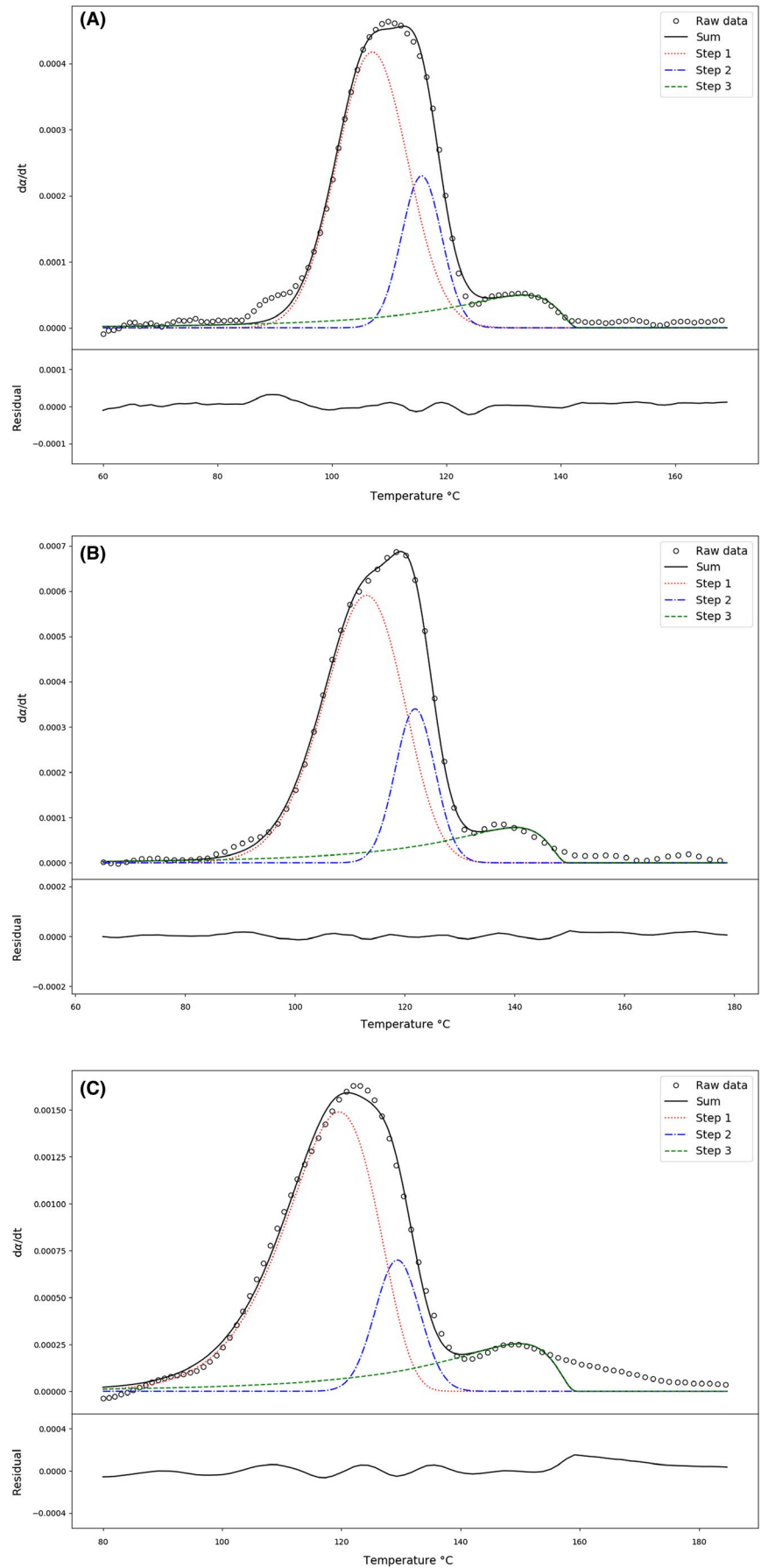
Beside the general scientific disagreement on the number of reaction steps (two or three), kinetic results in presented literature hitherto showed a variety of different kinetic results (Table 1). With respect to the impact on the reaction rate, there are various reasons for the wide range of published kinetic results, making the comparison of these results hardly feasible. So far, the missing of a clear separation of each reaction step is very likely one source of error. For overlapping reactions, the change in the activation energy mainly depends on the contribution of each reaction step, leading to a variation of the activation energy.

In addition to that, Khawam⁴² also described other factors, with influence on the kinetic of a heterogeneous reaction. Solid-state samples strongly interact with surrounding particles during a reaction. Therefore, with increasing reaction progress the reactivity could change as well due to product formation, crystal defect formation, intra-crystalline strain, or other effects. Furthermore, experimental variables affecting the heat or mass transfer at a reaction interface could also cause a reactivity change, placing high-quality requirements on the experimentally determined data, such as ensuring the heating rate to be the only variable for non-isothermal experiments.⁴² Without identical experimental conditions and sample material as well as a clear separation of the respective reaction steps, a comparison of the kinetic results remains generally inconclusive.

This work's methodology combines the deconvolution procedure, enhanced by stoichiometric information for the evaluation of the obtained results, with subsequent kinetic analysis via the NPK method. The main purpose of the deconvolution, first proposed by Perejon et al.,²⁷ is to obtain the individual rate peaks of the single reaction steps thus, enabling the subsequent kinetic analysis of each reaction step.³³ Within this work, experimental thermogravimetric data, consisting of overlapped rate peaks, were deconvoluted and the results were analyzed for the two different proposed reaction sequences in consideration of the stoichiometric information.

These work findings revealed that the boric acid decomposition is more likely to consist of three than two reaction steps. A three-step reaction can more suitably describe the decomposition reaction, whereas in literature, often-proposed two-step reaction does not take into account the stoichiometric-related mass loss of the decomposition reaction (Figure 10).

FIGURE 11 Deconvolution results, assuming a three-step reaction ($r > 99\%$); reaction ratios for heating rates of: (A) $2^\circ\text{C}/\text{min}$ of 67:14:19%, (B) $4^\circ\text{C}/\text{min}$ of 67:19:14% and (C) $8^\circ\text{C}/\text{min}$ of 64:19:17%



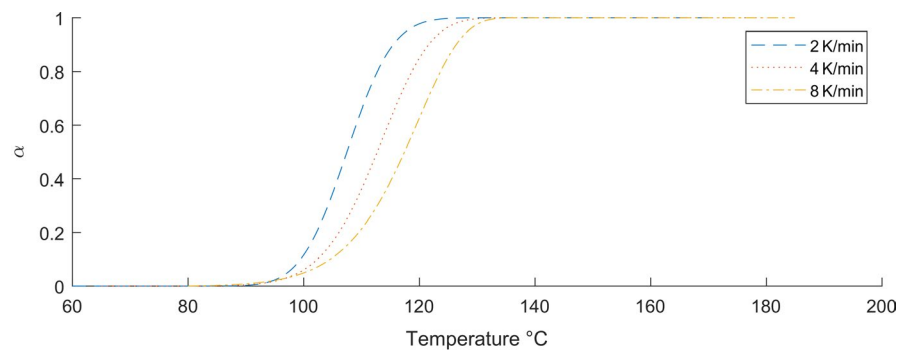


FIGURE 12 Conversion and conversion rate calculated for unfolded reaction step 1 at heating rates of 2, 4, and 8 C/min

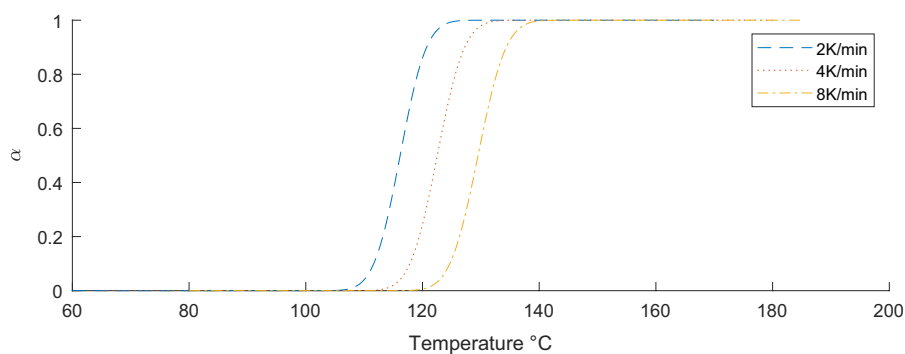
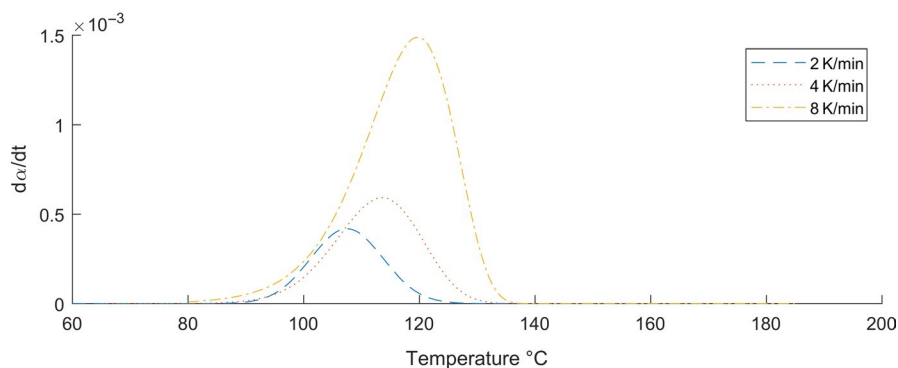
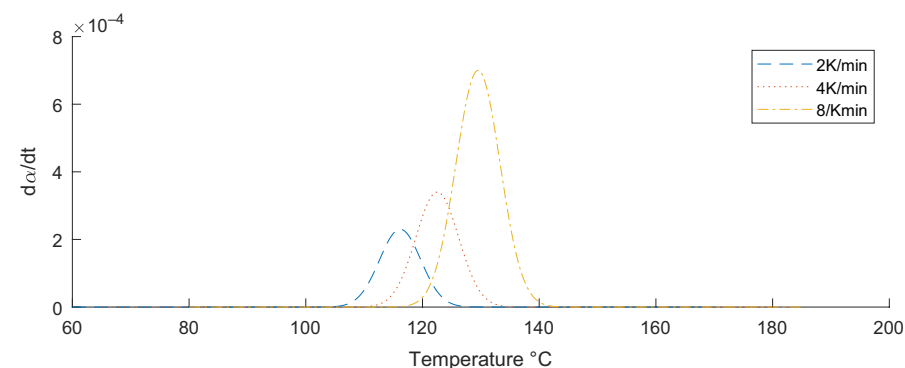


FIGURE 13 Conversion and conversion rate, calculated for unfolded reaction step 2 at heating rates of 2, 4, and 8 C/min



The kinetic analyses of the individual reaction steps were performed for the first time by means of the nonparametric kinetics 2 (NPK2) method followed by an analysis of the kinetic triplet (Figure 1). The first reaction step (step 1) could be described either by a reaction order model or by a diffusion model with an activation energy of 193.3 kJ/mol. The diffusion mechanism was already identified in earlier works, suitable for describing the first reaction step.²¹ The higher deviations in this region are mathematically

caused by the baseline fit. Hence, the algorithm failed to clearly unfold the overall curve at the reaction start, causing significant data uncertainties. However, the weighted results ensured that these uncertainties did not affect the model identification, which is why there are various fitting models.

Nucleation models can reasonably describe the second reaction step (step 2) with an activation energy of 117.6 kJ/mol. This step is overlapped and apparently highly influenced

FIGURE 14 Conversion and conversion rate, calculated for unfolded reaction step 3 at heating rates of 2, 4, and 8 C/min

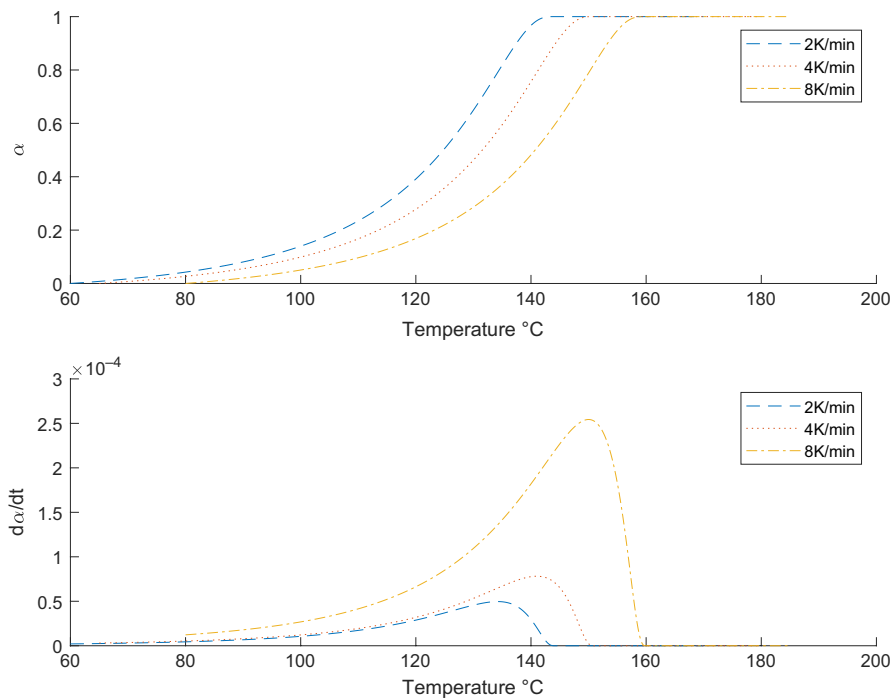
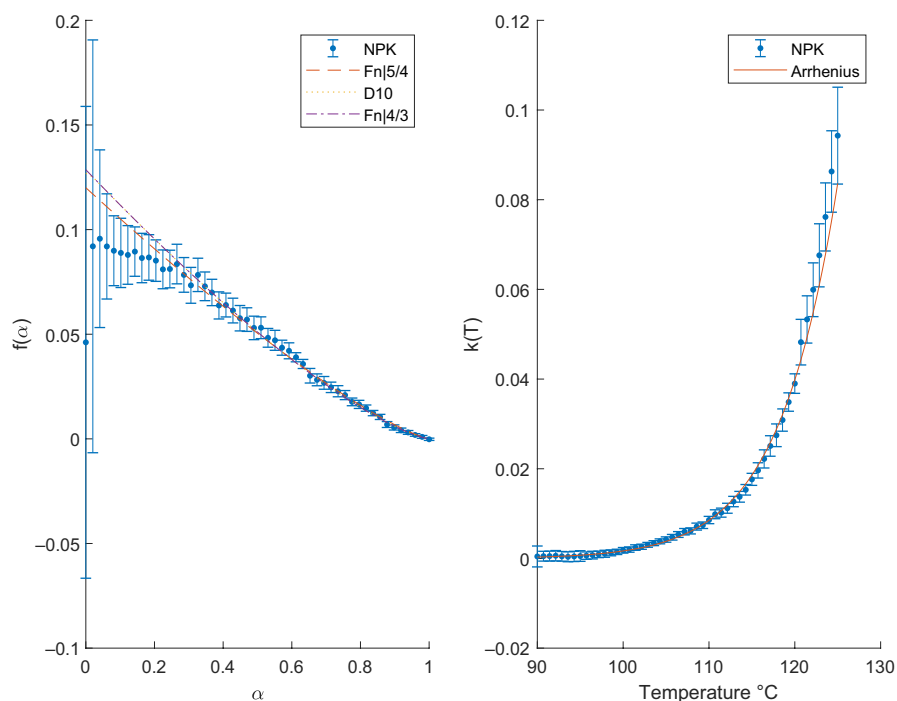


FIGURE 15 Generated models from NPK method and best fitted model to experimental data (left); temperature dependences of data (right) calculated for step 1



by step 1 and 3 causing a higher deviation and an oscillating behavior of the reaction's conversion and temperature dependency.

The last reaction step (step 3) is best described by a diffusion model with an activation energy of 149.6 kJ/mol. This mechanism would correspond to the results of Zhang et al.²¹

SEM analysis showed structural surface changes during the reaction. This insight was confirmed by the XRD analysis, performed after the thermal treatment, revealing the

change toward an amorphous structure (eg, by melting). In literature, several reactions are described to be accompanied by melting due to the influence of an intermediate product.¹⁸ This would correspond to the macroscopic investigation results under thermal exposure. The formation of a tablet from single particles was observed while using a low-temperature ramp of 2°C/min and a holding temperature of 155°C, much lower than the actual melting temperature of boric acid (171°C) or boron oxide (>325°C).

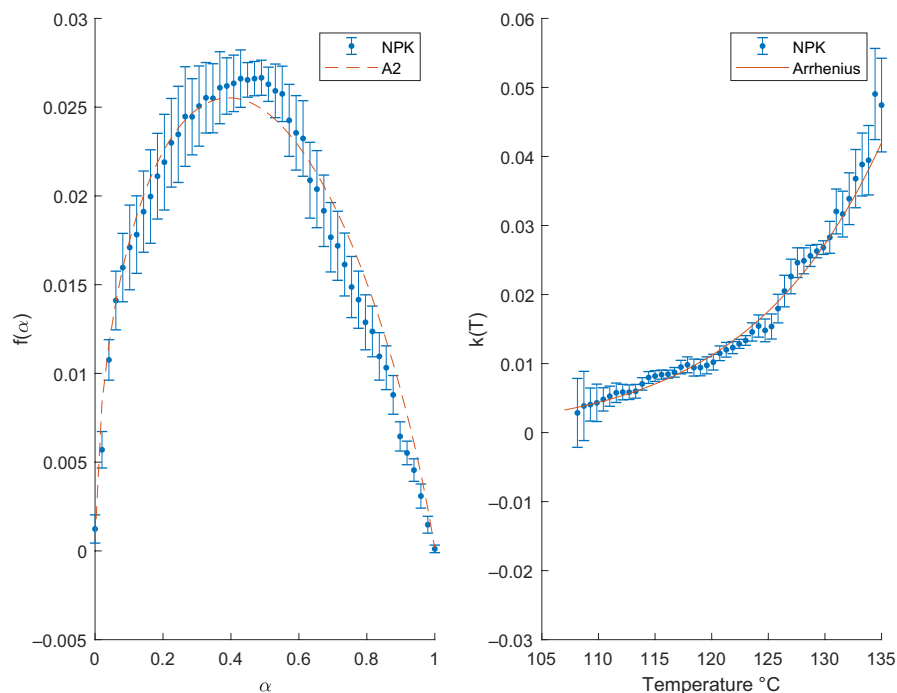


FIGURE 16 Generated models from NPK method and best fitted model to experimental data (left); temperature dependences of data (right) calculated for step 2

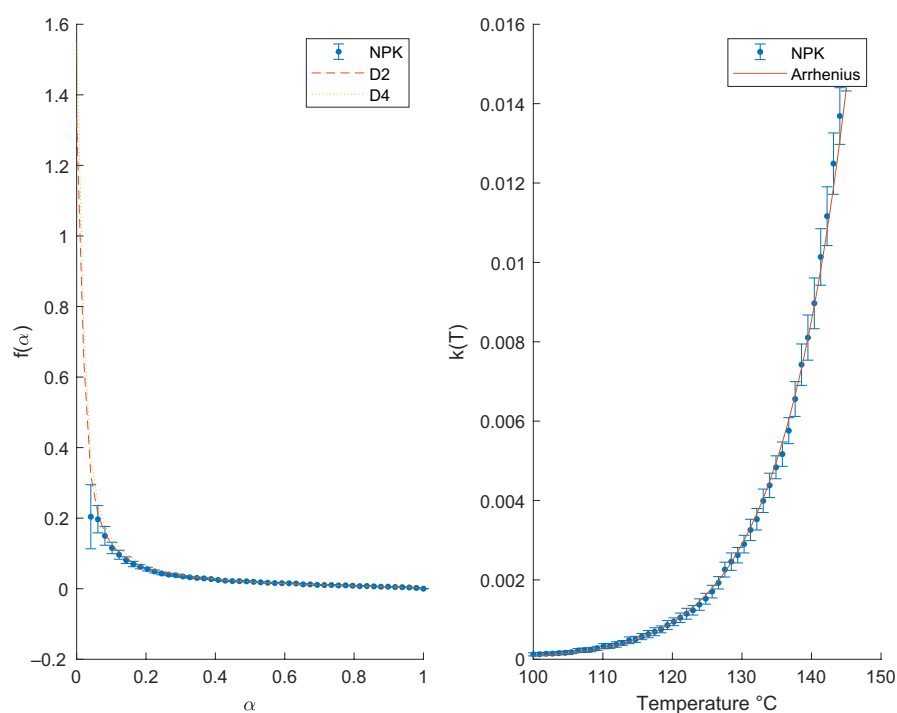


FIGURE 17 Generated models from NPK method and best fitted model to experimental data (left); temperature dependences of data (right) calculated for step 3

TABLE 4 Kinetic results for each reaction step

Reaction step	Reaction path	Model	A [1/s]	E_a [kJ/mol]	95% confidence interval of E [kJ/mol]
1	$\text{H}_3\text{BO}_3 > \text{HBO}_2$	Fn 5/4	2.3×10^{23}	193.3	(189.6, 197.0)
2	$\text{HBO}_2 > \text{H}_2\text{B}_4\text{O}_7$	A2	1.4×10^{12}	117.6	(113.3, 121.9)
3	$\text{H}_2\text{B}_4\text{O}_7 > \text{B}_2\text{O}_3$	D2	9.4×10^{14}	149.6	(148.0, 151.2)

However, since the results of kinetic analysis can only declare that a respective reaction step can be well described by a particular kinetic model, further investigations on this

reaction and the observed structural changes (like surface melting, sublimation¹⁰) with impact on the activation energy are still necessary to be confirmed. To address the issue of

TABLE 5 Best fitted models for reaction step 1

	Model	SSE	R ²	P (α = .05)
1	Fn 5/4	1.76 × 10 ¹	0.999	
2	D10	2.46 × 10 ¹	0.999	.123
3	Fn 4/3	2.46 × 10 ¹	0.999	.122
4	Fn 3/2	8.36 × 10 ¹	0.997	.000
5	Fn 1	1.16 × 10 ²	0.996	.000
6	F1	1.17 × 10 ²	0.996	.000

TABLE 6 Best fitted models for reaction step 2

	Model	SSE	R ²	P (α = 0.05)
1	A2	7.65 × 10 ¹	0.993	
2	A5	2.15 × 10 ²	0.980	.000
3	B1	2.56 × 10 ²	0.976	.000
4	A3	2.81 × 10 ²	0.974	.000
5	A1	4.79 × 10 ²	0.955	.000
6	A4	5.03 × 10 ²	0.953	.000

TABLE 7 Best fitted models for reaction step 3

	Model	SSE	R ²	P (α = .05)
1	D2	7.72 × 10 ¹	0.999	
2	D4	1.16 × 10 ²	0.998	.081
3	D8	2.21 × 10 ²	0.996	.000
4	F1	3.14 × 10 ²	0.994	.000
5	Fn 1	3.15 × 10 ²	0.994	.000
6	Fn 5/4	3.47 × 10 ²	0.994	.000

melting or other formation of amorphous phases below the melting temperature, further analyses on the decomposition under thermal exposure regarding the intermediates and their interaction are recommended.

ACKNOWLEDGMENTS

The authors thank the Austrian Research Promotion Agency (FFG) for the financial support of the project SolidHeat Kinetics (848876) and SolidHeat Pressure (853593). The X-Ray Center (CRC) of TU Wien is acknowledged for providing access to the powder X-ray diffractometers. Many thanks to the Mechanical Engineering and Clean Air Technology research group of the institute for Chemical, Environmental and Bioscience Engineering providing the Mastersizer 2000 for measuring the particle size distribution of samples and providing access to the SEM. The authors acknowledge the TU Wien University Library for financial support through its Open Access Funding Program.

CONFLICT OF INTEREST


The authors declare no conflict of interest.

AUTHOR CONTRIBUTIONS

Formal analysis, CH, and SSJ; Investigation, CH, SSJ and CJ; Methodology, CH, FB and SSJ; Project administration, MH, MS and FW; Resources, SSJ, MH, MS and FW; Software, CH, FB, JW and SSJ; Supervision, MH, MS and FW; Validation, SSJ and CJ; Visualization, CH; Writing—original draft, CH; Writing—review & editing, CH, SSJ, CJ, MS and FW CH involved in conceptualization, data curation, visualization, and writing original draft; CH and SSJ involved in formal analysis; CH, SSJ, and CJ investigated; CH, FB, and SSJ involved in methodology; MH, MS, and FW involved in project administration; SSJ, MH, MS, and FW involved in resources; CH, FB, JW, and SSJ involved in software; MH, MS, and FW supervised; SSJ and CJ validated; CH, SSJ, CJ, MS, and FW reviewed and edited.

ORCID

Clemens Huber  <https://orcid.org/0000-0001-8823-6955>

Saman Setoodeh Jahromy  <https://orcid.org/0000-0003-4395-4181>

Felix Birkelbach  <https://orcid.org/0000-0003-4928-6209>

Manfred Schreiner  <https://orcid.org/0000-0002-0870-1827>

Michael Harasek  <https://orcid.org/0000-0002-6490-5840>

Franz Winter  <https://orcid.org/0000-0001-9854-3836>

REFERENCES

1. Global Footprint Network. *Ecological Footprint*. <https://www.footprintnetwork.org/our-work/ecological-footprint/>. Accessed March 06, 2019.
2. International Energy Agency. *World Energy Outlook 2017*; 2017.
3. United Nations. *Secretary-General Urges Governments to Take Long-term View on Renewable Energy, Spelling Out Priorities at 'Clean Industrial Revolution' Event in Durban*. <https://www.un.org/press/en/2011/sgsm13998.doc.htm>. Accessed March 07, 2019.
4. Gonzalez-Roubaud E, Perez-Osorio D, Prieto C. Review of commercial thermal energy storage in concentrated solar power plants: steam vs. molten salts. *Renew Sust Energ Rev*. 2017;80:133-148.
5. Alva G, Lin Y, Fang G. An overview of thermal energy storage systems. *Energy*. 2018;144:341-378.
6. Scorei RI, Rotaru P. Calcium fructoborate—potential anti-inflammatory agent. *Biol Trace Elem Res*. 2011;143:1223-1238.
7. Iavazzo C, Gkegkes ID, Zarkada IM, Falagas ME. Boric acid for recurrent vulvovaginal candidiasis: the clinical evidence. *J Womens Health (Larchmt)*. 2011;20:1245-1255.
8. Perelygin YP, Chistyakov DY. Boric acid. *Russ J Appl Chem*. 2006;79:2041-2042.
9. U.S. Geological Survey. *Mineral Commodity Summaries 2018*; U.S. Department of the Interior: 31.01.2018; 2018.

10. Huber C, Setoodeh Jahromy S, Jordan C, et al. Boric acid: a high potential candidate for thermochemical energy storage. *Energies*. 2019;12:17.
11. Pardo P, Deydier A, Anxionnaz-Minvielle Z, Rouge S, Cabassud M, Cognet P. A review on high temperature thermochemical heat energy storage. *Renew Sust Energ Rev*. 2014;32:591-610.
12. Kracek F, Morey G, Merwin H. The system, water-boron oxide. *Am J Sci A*. 1938;35:143-171.
13. Mukhanov VA, Kurakevich OO, Solozhenko VL. On the hardness of boron (III) oxide. *J Superhard Mater*. 2008;30:71-72.
14. Dressler W. *Ueber die Flüchtigkeit der Borsäure. neue Bestimmungen des Verteilungsgleichgewichtes zwischen Wasser und Dampf*. ETH Zürich; 1945.
15. Zachariassen WH. The crystal structure of cubic metaboric acid. *Acta Crystallogr A*. 1963;16:380-384.
16. Napolitano A, Macedo PB, Hawkins EG. Viscosity and density of boron trioxide. *J Am Ceram Soc*. 1965;48:613.
17. Weir RJ, Fisher RS. Toxicologic studies on borax and boric-acid. *Toxicol Appl Pharmacol*. 1972;23:351.
18. Galwey AK. Thermal-reactions of selected solids including reactants that melt during chemical-change. *J Therm Anal*. 1994;41:267-286.
19. Sevim F, Demir F, Bilen M, Okur H. Kinetic analysis of thermal decomposition of boric acid from thermogravimetric data. *Korean J Chem Eng*. 2006;23:736-740.
20. Balcı S, Sezgi NA, Eren E. Boron oxide production kinetics using boric acid as raw material. *Ind Eng Chem Res*. 2012;51:11091-11096.
21. Zhang W, Sun S, Xu J, Chen Z. Kinetic study of boron oxide prepared by dehydration of boric acid. *Asian J Chem*. 2015;27:1001-1004.
22. Harabor A, Rotaru P, Scorei RI, Harabor NA. Non-conventional hexagonal structure for boric acid. *J Therm Anal Calorim*. 2014;118:1375-1384.
23. Rotaru A. Thermal and kinetic study of hexagonal boric acid versus triclinic boric acid in air flow. *J Therm Anal Calorim*. 2017;127:755-763.
24. Aghili S, Panjepour M, Meratian M. Kinetic analysis of formation of boron trioxide from thermal decomposition of boric acid under non-isothermal conditions. *J Therm Anal Calorim*. 2018;131:2443-2455.
25. Alvarez-Valdes JG, Pico Marin C, Gutierrez Rios E. the thermal decomposition mechanism of orthoboric acid. *Anales de Química*. 1978;74:724-726.
26. Vyazovkin S, Burnham AK, Criado JM, Pérez-Maqueda LA, Popescu C, Sbirrazzuoli N. ICTAC Kinetics Committee recommendations for performing kinetic computations on thermal analysis data. *Thermochim Acta*. 2011;520:1-19.
27. Perejon A, Sanchez-Jimenez PE, Criado JM, Perez-Maqueda LA. Kinetic analysis of complex solid-state reactions. A new deconvolution procedure. *J Phys Chem B*. 2011;115:1780-1791.
28. Wang Y, Wen J, Wang T, et al. Synthesis of $(\text{La}_{0.8}\text{Y}_{0.2})\text{PO}_4$: Sm^{3+} , Eu^{3+} , Na^+ and kinetics mechanism study with $Z(\alpha)$ master plots method for thermal process of its precursor. *J Therm Anal Calorim*. 2019;136:2487-2494.
29. Birkelbach F, Deutsch M, Flegkas S, Winter F, Werner A. NPK 2.0: introducing tensor decompositions to the kinetic analysis of gas-solid reactions. *Int J Chem Kinet*. 2019;51:280-290.
30. Vyazovkin S, Chrissafis K, Di Lorenzo ML, et al. ICTAC Kinetics Committee recommendations for collecting experimental thermal analysis data for kinetic computations. *Thermochim Acta*. 2014;590:1-23.
31. Khawam A, Flanagan DR. Solid-state kinetic models: basics and mathematical fundamentals. *J Phys Chem B*. 2006;110:17315-17328.
32. Koga N, Malek J, Sestak J, Tanaka H. Data treatment in non-isothermal kinetics and diagnostic limits of phenomenological models. *Netsu Sokutei*. 1993;20:210-223.
33. Vyazovkin S, Koga N, Schick C. *Handbook of Thermal Analysis and Calorimetry: Recent Advances, Techniques and Applications*, Vol. 6. Elsevier; 2018.
34. Koga N, Goshi Y, Yamada S, Pérez-Maqueda LA. Kinetic approach to partially overlapped thermal decomposition processes. *J Therm Anal Calorim*. 2013;111:1463-1474.
35. Hu M, Chen Z, Wang S, et al. Thermogravimetric kinetics of lignocellulosic biomass slow pyrolysis using distributed activation energy model, Fraser-Suzuki deconvolution, and iso-conversional method. *Energy Convers Manage*. 2016;118:1-11.
36. Svoboda R, Málek J. Applicability of Fraser-Suzuki function in kinetic analysis of complex crystallization processes. *J Therm Anal Calorim*. 2012;111:1045-1056.
37. Savitzky A, Golay MJ. Smoothing and differentiation of data by simplified least squares procedures. *Anal Chem*. 1964;36:1627-1639.
38. Serra R, Nomen R, Sempere J. The non-parametric kinetics a new method for the kinetic study of thermoanalytical data. *J Therm Anal Calorim*. 1998;52:933-943.
39. Setoodeh Jahromy S, Birkelbach F, Jordan C, et al. Impact of partial pressure, conversion, and temperature on the oxidation reaction kinetics of Cu_2O to CuO in thermochemical energy storage. *Energies*. 2019;12:508.
40. Brown ME. *Introduction to Thermal Analysis*. 2004.
41. Griva I, Nash SG, Sofer A. *Linear and nonlinear optimization*, Vol. 108. Siam. 2009.
42. Khawam A. *Application of Solid-state Kinetics to Desolvation Reactions*. University of Iowa; 2007.
43. Dickinson CF, Heal GR. Solid-liquid diffusion controlled rate equations. *Thermochim Acta*. 1999;340-341:89-103.

How to cite this article: Huber C, Jahromy SS, Birkelbach F, et al. The multistep decomposition of boric acid. *Energy Sci Eng*. 2020;8:1650–1666. <https://doi.org/10.1002/ese3.622>